RSC Advances

PAPER

View Article Online
View Journal | View Issue

Cite this: RSC Adv., 2014, 4, 33262

Fast photocatalytic degradation of congo red using CoO-doped β-Ga_2O_3 nanostructures†

Minoo Bagheri,[a] Ali Reza Mahjoub,*[a] Abbas Ali Khodadadi*[b] and Yadollah Mortazavi[c]

In this investigation, the influence of cobalt(II) oxide on the photocatalytic activity of Ga_2O_3 rod-like nanostructures in the presence of 30 ppm congo red is studied. Samples of Ga_2O_3 doped with 1, 2, 3 and 5 wt% CoO were synthesized by employing a facile co-precipitation method using aqueous solutions of Co(II) chloride and gallium nitrate and CTAB as a structure directing agent and characterized by X-ray diffraction, energy-dispersive X-ray, scanning electron microscopy, photoluminescence, BET surface area, UV-vis diffuse reflectance spectroscopy and point of zero charge techniques. The samples containing up to 2 wt% of CoO calcined at 900 °C revealed that only a monoclinic structure of Ga_2O_3 is formed. Despite equal phase of β-Ga_2O_3, two other phases of $CoGa_2O_4$ and α-Ga_2O_3 were observed in X-ray diffraction patterns of samples containing 3 and 5 wt% of CoO, respectively. UV-vis diffuse reflectance spectroscopy showed a significant reduction in band gap upon increasing their CoO content, indicating incorporation of CoO in the gallia lattice. The sample containing 3 wt% CoO–Ga_2O_3 can remove 30 ppm of congo red readily within 75 minutes and it exhibited a high photo-degradation activity of about 82.5% after 80 h of irradiation. These results suggest that CoO–gallia/UV photocatalysis may be envisaged as a method for treatment of diluted colored waste water not only for decolorization, but also for detoxification in textile industries. The photocatalytic degradation of the dye in solution obeys first order reaction kinetics.

Received 18th May 2014
Accepted 15th July 2014

DOI: 10.1039/c4ra04668d

www.rsc.org/advances

Introduction

In recent years, worldwide attention to environmental problems has continued to increase. Unfortunately, use of synthetic dyes (such as azo dyes), especially in the textile industries, and discharge of waste containing these toxic compounds into aquatic systems are considered as environmental threats among the researchers in this field.[1–3] Azo dyes, consisting of azo bonds (–N=N–) as chromophores, are a well-known class of dyes, which are highly toxic and even carcinogenic to animals and humans, and are not readily degradable.[4]

Due to their complicated aromatic structures, diazo dyes (*e.g.*, Congo red (CR) (sodium salt of benzidinediazobis-1-naphthylarnine-4-sulfonic acid)) are thermally and optically stable, and thus difficult to decompose.[5] However, photocatalytic decomposition of such pollutants is a clean and repeatable way to decrease their harmful effects.[5,6]

Metal oxide semiconductor (MOS) materials, because of their special properties, have been used for various applications such as electronics, optics, thermoelectronics and photoelectronics. It is interesting to note that type, morphology, size, and structure of MOSs play a major role in the characteristics of these materials. Therefore, by controlling the synthesis parameters, it becomes possible to prepare these oxides with specific properties suitable for particular applications.[7,8]

Among the MOSs, which are employed as photocatalysts, β-Ga_2O_3 is a new environmentally friendly material that possesses a much wider band gap (4.8 eV)[9] relative to that of TiO_2 (3.2 eV).[10] This feature leads to the enhancement of the mobility of photo-generated electrons and the promotion of charge separation.[11] The positions of conduction bands (CB) of β-Ga_2O_3 and TiO_2 are at −2.95 eV (ref. 12) and −4.21 eV,[9] respectively. Thus, the photo-generated electrons in the CB of β-Ga_2O_3 have much higher reductive capability than those of TiO_2. In addition, the photo-generated electrons in the sp hybridized band of gallium (Ga: 4s4p) have high mobility owing to large band dispersion.[13] The higher mobility of photo-generated electrons will improve the separation efficiency of photo-generated holes and electrons. Therefore, deactivation of the catalyst should not cause much concern.[13]

In order to improve the photocatalytic efficiency of MOSs, various modifications have been carried out such as: (a) surface modification by means of noble metals or coupling with other semiconductors, (b) sensitization through the narrow band gap semiconductors or organic dyes, and (c) doping the ions with other metal and non-metal ions.[14–17] The p–n diode-type

[a]Department of Chemistry, Tarbiat Modares University, Tehran, Iran. E-mail: mahjouba@modares.ac.ir; Fax: +98 21 82883455; Tel: +98 21 82883442

[b]Catalysis and Nanostructured Materials Research Laboratory, School of Chemical Engineering, University of Tehran, Tehran, Iran. E-mail: khodadad@ut.ac.ir; Fax: +98 21 66967793; Tel: +98 21 6696 7793

[c]Nanoelecronics Center of Excellence, University of Tehran, Tehran, Iran

† Electronic supplementary information (ESI) available. See DOI: 10.1039/c4ra04668d

photocatalysts have attracted much attention in recent years.[18] Cobalt oxide CoO is p-type semiconductor with a band gap energy at around 2.4 eV (ref. 19) and interesting electronic and magnetic properties[20] that may be attractive and suitable to photodegradation of organic pollutants.[18]

In this work, our strategy relies on the effect of CoO on gallia photocatalytic activities. We herein report synthesis of CoO-doped Ga_2O_3 nanostructures for photodegradation of 30 ppm congo red. The photocatalytic activity of the samples substantially changed with their CoO content.

Experimental

Reagents and chemicals

Analytical grade Cobalt(II) chloride hexahydrate ($CoCl_2 \cdot 6H_2O$, Aldrich), absolute ethanol, and gallium nitrate hydrate ($Ga(NO_3)_3 \cdot xH_2O$, Aldrich) were purchased and employed without further purification. The number of water molecules, "*x*", in $Ga(NO_3)_3 \cdot xH_2O$ was determined by thermogravimetric analysis (TGA), and found to be 8. The CR (purity 99%, Aldrich) was used as received.

Synthesis of materials

Synthesis of CoO-doped β-Ga_2O_3 nanostructures. First, a proper amount of CTAB was dissolved in 20 ml double distilled water; so that the mass ratio of the gallia precursor to CTAB was 10 : 1 in all the samples. Afterwards, $Ga(NO_3)_3 \cdot 8H_2O$ and m (g) of $CoCl_2 \cdot 6H_2O$ were added into the solution to acquire the needed percentages of CoO (0, 1, 2, 3 and 5 wt%). After 10 min of vigorous stirring, a 1 M NH_4OH solution was added to the mixture to adjust the pH at about 9. A cloudy mixture was formed, which was kept at 60 °C for 7 h. The white/violet precipitate was separated, washed with double distilled water, dried at 60 °C under vacuum and eventually calcined at 900 °C for 2 h. The samples were denoted as GC-*x*, wherein "*x*" specifies the percentage of CoO.

Characterization. The size and morphology of the β-Ga_2O_3 nanostructures were observed *via* the scanning electron microscopy (SEM) at an accelerating voltage of 17.0 kV by a Philips XL30 microscope (The Netherlands) while the field emission scanning electron microscopy (FESEM) at an accelerating voltage of 20.0 kV by a ZEISS SIGMA VP microscope was used for CoO-loaded β-Ga_2O_3 samples (German). The energy dispersive X-ray (EDX) analysis was performed by the same microscopes to examine the elemental compositions of the samples. The wide-angle X-ray diffraction (XRD) patterns of the oxide powders were recorded on a Philips Xpert diffractometer (The Netherlands) using Cu Kα radiation (λ = 1.5418 Å) to identify the crystalline phases. The specific surface areas (SSA) of the nanocomposites were determined by nitrogen adsorption through a CHEM-BET 3000 instrument using the Brunauer–Emmett–Teller (BET) equation. Prior to the SSA measurements, the samples were degassed for 0.5 h at 300 °C at atmospheric pressure. The photoluminescence (PL) spectra were recorded by means of a Perkin-Elmer LS-5 luminescence spectrometer with an excitation wavelength of 290 nm at RT. The ultraviolet-visible diffuse reflectance spectra were recorded on an Avantes avaspec2048tec reflection probe (fcr-7uv400) using $BaSO_4$ as a reference. The surface charge densities and points of zero charge (PZC) of the samples were measured with the aid of a Zeta Pals Brookhaven (U.S.A.) instrument.

Evaluation of photocatalytic activity. The CR (C.I. Direct Red 28 $C_{32}H_{24}N_6O_6S_2 \cdot 2Na$) was chosen as model pollutant to evaluate the photocatalytic activity of the samples. The irradiation experiments of CR were carried out on stirred aqueous solutions in a cylindrical quartz UV reactor, containing about 50 ml of a 30 ppm aqueous CR solution, in presence of about 25 mg of the CoO–Ga_2O_3 photocatalyst. The suspension was sonicated for 5 min and subsequently stirred in the dark for 30–45 min (depending on the type of samples and their darkness time found based on the absorption experiments), to establish the adsorption/desorption equilibrium on the semiconductor surface before UV irradiation. The irradiation was done with a UV lamp (30 W, UV-C, λ = 253.7 nm, 4.89 eV, Philips (The Netherlands)). The temperatures of the samples did not exceed 20 °C, owing to the circulation of tap water in the jacket of the UV reactor. Perpendicular UV irradiation was applied when the distance between the UV source and the reaction mixture was almost 15 cm. Air was blown into the reaction mixture by an air compressor, to maintain the oxygen saturation in the solution during the course of reaction. Analytical samples were taken from the reaction suspension after specified reaction times, immediately centrifuged at 6000 rpm for 10 min to remove the particles, and further analyzed through monitoring their absorbance at 497 nm using an ultraviolet-visible (UV-Vis) spectrophotometer (Shimadzu UV 2100). The concentration of dye in each degraded sample was determined at λ_{max} = 497 nm, using the calibration curve. With this method, the percent removal of CR could be attained at different intervals. The percent removal was calculated by the following equation:

$$\%\ \text{Removal} = (C_i - C_t)/C_i \times 100 \quad (1)$$

where, C_i is the initial concentration of dye and C_t is the concentration of dye at any given time.

To scrutinize the impact of pH on the removal of CR, the pH of the dye solution was altered (in the range of 4–9) by adding incremental amounts of 0.1 M HCl/NaOH. Extra studies were conducted on the CR dye at an optimum adjusted initial pH.

The chemical oxygen demand (COD) test is extensively employed as an effective technique to measure the organic strength of wastewater. This test allows measurement of waste in terms of the total quantity of oxygen required for oxidation of organic matter to CO_2 and water. In the present work, the open reflux method was used for COD determination.[21]

The photocatalyst stability tests were carried out in the same way as the photocatalytic activity tests, but repeated four times.

Results and discussion

Characterization of CoO-doped β-Ga_2O_3 nanostructures

The results of elemental analyses of the samples, determined by EDX, are in good agreement with the nominal compositions of the samples (Fig. S1† and Table 1).

Table 1 EDX analysis, BET surface areas, crystallinity, band gap and photocatalytic properties of the samples

Samples	Ga (wt%)	Co (wt%)	T_{dark} (min)	$T_{Removal}$ (min)	% Removal	Band gap (eV)	BET area (m^2 g^{-1})	Crystallinity (%)
G	100	—	20	120	59.4	4.96	31.5	68.5
GC-1	98.8	1.2	20	120	62.5	4.8	38.1	—
GC-2	97.5	2.5	20	120	75.2	4.7	40.2	66.5
GC-3	96.4	3.6	30	75	99.7	4.6	51.3	55.1
GC-5	94.7	5.3	30	90	99.5	4.5	55.4	43.6

The SSA of the samples, comprising various proportions of CoO, is listed in Table 1. It is evident from Table 1 that the surface areas of the samples are enhanced upon adding more cobalt(II) oxide to gallia. A sharp increase in the SSA is observed for the sample containing 3 wt% of CoO.

Fig. 1 depicts the X-ray diffraction (XRD) patterns of the samples. As seen in Fig. 2, for these samples, containing 0–2 wt% CoO and calcined at 900 °C, the Bragg diffraction peaks (in the range of $2\theta = 20°–80°$) exhibit the typical patterns of a monoclinic structure of β-Ga_2O_3, which is consistent with the reported data by the JCPDS card no. 43-1012, with lattice parameters of $a = 12.23$, $b = 3.04$, $c = 5.80$ Å, and $\beta = 103.7°$. In the XRD patterns of the samples, with 0–2 wt% CoO, no peak can be assigned to any known phase of CoO, probably because of the low content of CoO and/or small crystallite sizes not detected in the XRD patterns. For GC-3 sample, not only the β-Ga_2O_3 phase but also a few reflections of $CoGa_2O_4$ mixed metal oxide, with cubic structure and lattice parameter of $a = 8.325$ Å (JCPDS file no. 11-0698), are observed. In the case of GC-5 sample, two phases of gallium oxide (α and β) are observed.

The crystallinity of the samples is determined by the ratio of the crystalline area to the total area of each XRD pattern. As shown in Table 1, the crystallinity decreases upon adding cobalt(II) oxide to gallia so that the sample containing 5 wt% CoO has the lowest crystallinity among GC samples. Co^{2+} probably does not substitute for Ga^{3+}, due to having an ionic radius greater than that of Ga^{3+},[22] and the stoichiometry of the gallia may deteriorate because of the excess O and the incorporation of the CoO in the composed samples. Moreover, CoO can act as crystal growth inhibitor resulting in lower crystallinity of the samples. Similar behavior was observed for some metal oxides.[23–25]

The PL spectra of the samples containing 0, 1, 3 and 5 wt% cobalt(II) are displayed in Fig. 2. The PL spectrum of the pure Ga_2O_3 consists of one broad band, comprising some Gaussian bands centered at around 373, 414, 447 and 496 nm, which is ascribed to the recombination of an electron on a donor (oxygen vacancies) and a hole on each acceptor (gallium–oxygen vacancy pairs).[26] The band intensity appreciably decreases, which can be attributed to a decline in recombination rate of electron–hole pairs in GC samples.

As a result, BET values (increasing in SSA upon adding CoO) relate to decline in the particle size and/or increase in surface defects. PL spectra show no increase in peak intensity related to surface defects such as O-vacancies. Consequently, CoO can act as crystal growth inhibitor and increase SSA due to a decrease in particle size of the samples.

Morphologies of the samples, (both dried and calcined at 900 °C), were recorded using the SEM. The images are illustrated in Fig. 3(a–c) for G, GC-3 and GC-5, respectively. The morphology of the G sample is like a collection of attached sheets creating rod-like structures (Fig. 3a). The sheet-like structures exhibit an average length of 1.5 μm. In the case of GC-3 (Fig. 3b) the morphology is transformed from sheets into wheatear-like structures. The GC-5 is composed of attached wheatear-like structures which create spindle-like structures with a decline in the particle size of the sample.

Some of the UV-vis DRS spectra of the samples are displayed in Fig. 4a. The optical band gaps of the samples are estimated by

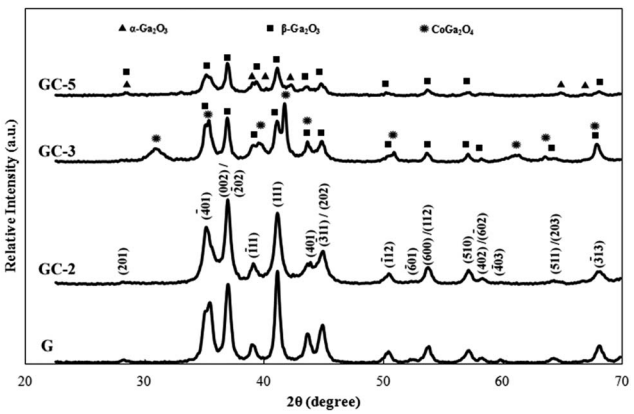

Fig. 1 XRD patterns of (0–5 wt%) CoO–Ga_2O_3 samples calcined at 900 °C for 2 h.

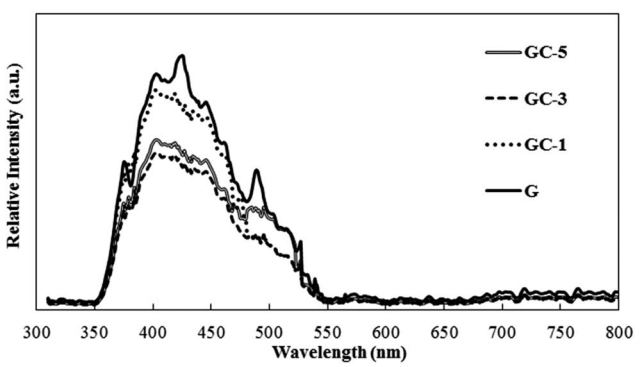

Fig. 2 PL spectra of G, GC-1, GC-3 and GC-5 samples.

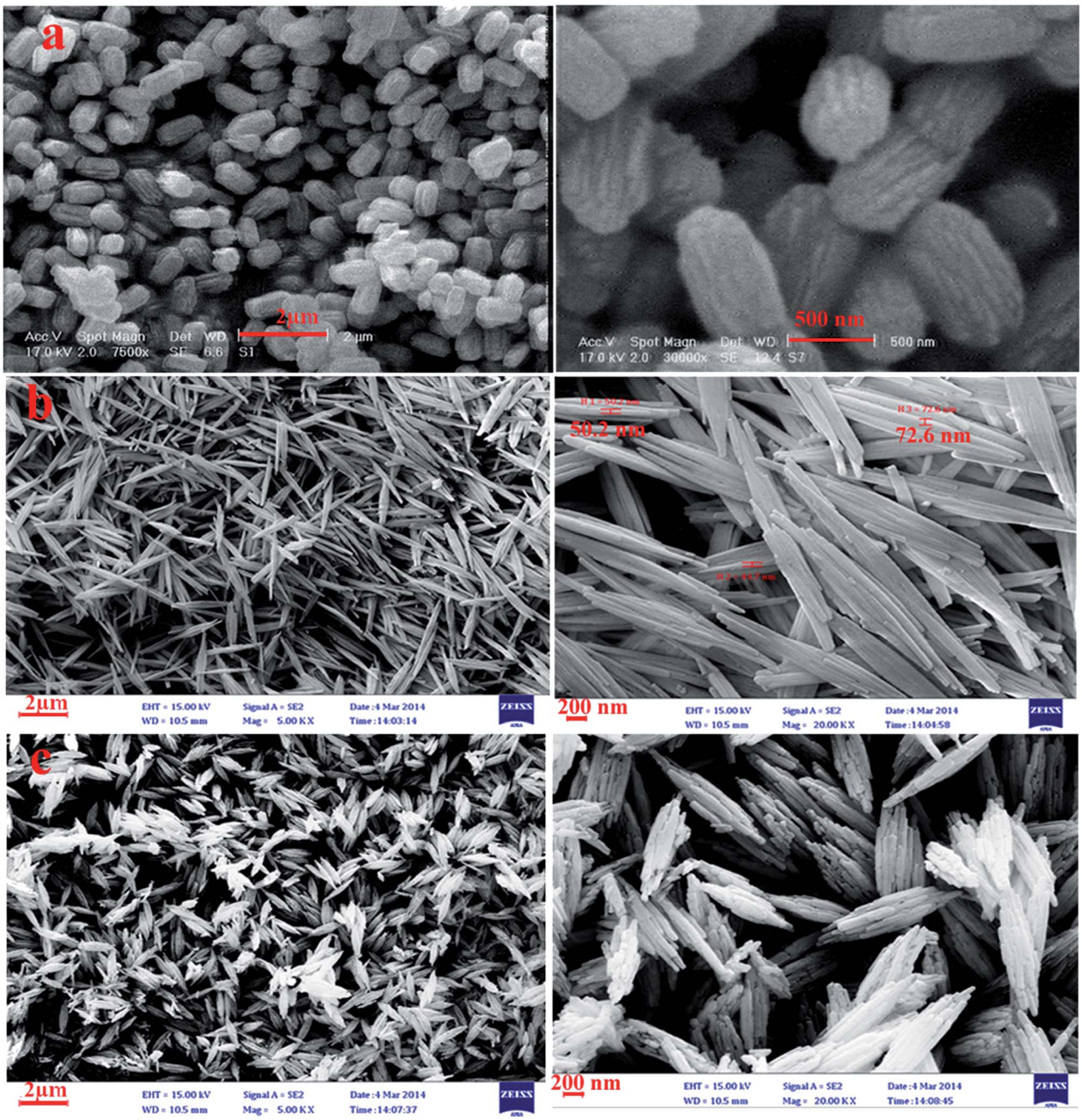

Fig. 3 SEM images of: (a) G, (b) GC-3 and (c) GC-5 samples (2 μm and 500/200 nm scales).

extrapolating the linear portion of the square of absorption coefficient against photon energy using the equation below:[27]

$$(\alpha h\nu)^2 = B(h\nu - E_g) \quad (2)$$

wherein B is a constant. Fig. 4b depicts the $(\alpha h\nu)^2$ *versus* photon energy ($h\nu$) plots of the above-mentioned samples. As seen in Fig. 4a, pure gallia exhibits a strong absorption in the short-UV region at approximately 250 nm with an optical band gap at roughly 4.96 eV, which is slightly larger than the values reported in previous works.[9,27]

This is due to the absorption of light caused by the excitation of electrons from the VB to the CB of gallia[28] (Table 1). The results indicate that addition of CoO has significant effect on gallia band gap. This may indicate that CoO may be doped to gallium oxide phase. These results are also in accordance with the results of XRD and PL. From G to GC-5 samples the decrement of band gap is at about 0.46 eV which is smaller than that of pure gallia. This is analogous to the findings for Sm_2O_3–ZnO in our previous study.[29]

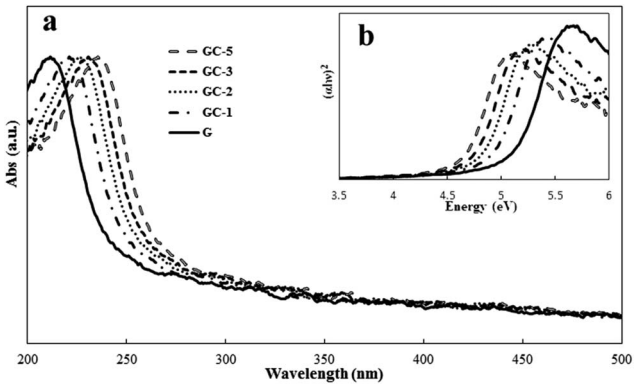

Fig. 4 (a) Optical absorption spectra of the 0, 1, 2, 3 and 5 wt% CoO–Ga_2O_3 samples and (b) $(\alpha h\nu)^2$ *versus* photon energy plots of the mentioned samples.

Photocatalytic activity

Effect of pH on removal of dye. Fig. 5a presents the removal efficiency *versus* pH (4–9) measured at 30 ppm concentration of CR under UV irradiation for 2 h at RT for G and GC-3 samples. The adsorption percentage of CR was increased by decreasing the pH to acidic range. Raising the pHs of solutions up to 8–9 caused the opposite and no adsorption was detected at pH of 9.

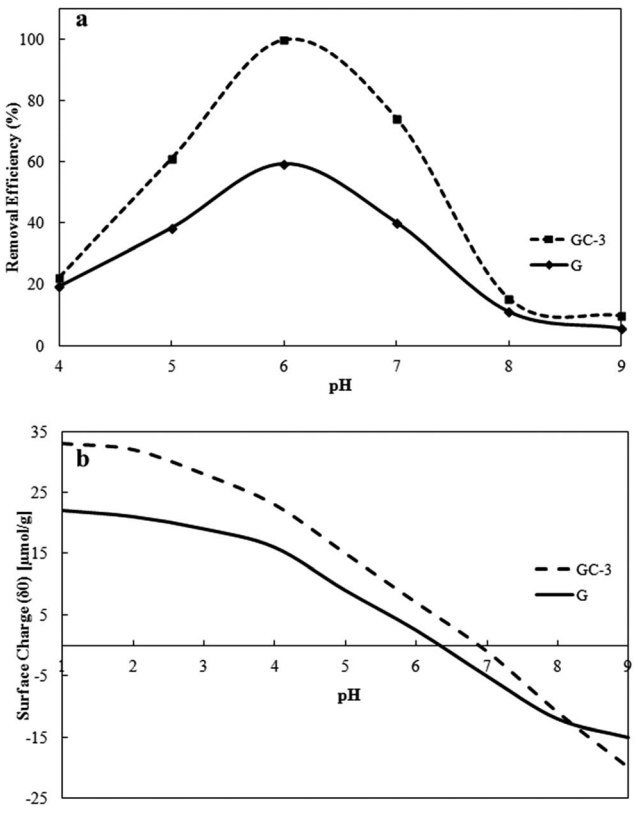

Fig. 5 Removal efficiency percentage *versus* pH for (a) G and GC-3 samples, condition: 0.025 g photocatalyst, 20 ml of CR dye with 30 ppm concentration, irradiation time 2 h at room temperature. (b) The δ0–pH curves for G and GC-3 samples.

The maximum removal efficiency of CR dye occurs at pH of 6. Accordingly, the pHs of all other solutions with various percentages of cobalt(II) oxide were adjusted to an optimum pH of 6 to improve the performance of adsorbent.

The surface charge data plotted as the δ0–pH curves for the G and GC-3 samples are depicted in Fig. 5b. As seen in this figure, in the pH range of 4–9, there is a linear decrease in surface charge with pH, which is subsequently followed by a sharp decline at pH level of about 9 for both samples. Furthermore, the surface charge densities, PZC values, increase with a rise in the CoO content of the samples. PZC values, determined from the δ0–pH curves, are 6.3 and 6.9 for the G and GC-3 samples, respectively.

With regard to the PZC of photocatalyst surface and the nature of dye (cationic, anionic, or neutral), pH of solution has a significant impact upon the adsorption efficiency of dye on the adsorbent surface. In pHs < PZC, the adsorbent surface is positively charged and owing to the anionic nature of CR, the electrostatic attraction leads to dye adsorption and the improvement of removal efficiency of CR; while in pHs > PZC, the surface is negatively charged,[30] and so the electrostatic repulsion is enhanced and the removal efficiency of CR is reduced. Another explanation for the effect of acidic pHs has also been reported which is based on the existence of hydrogen bonds between the photocatalyst's hydroxyl groups and the sulfonate or amine sites of dye molecules.[31] As the pH of CR solution increases, an extreme decrease in adsorption takes place. Normally, at higher pHs, the OH^- anion can compete with the anionic sites of CR dye and be adsorbed onto the positively charged groups of photocatalyst, which in turn results in the blocking of activated sites.[31]

Effect of CoO content on CoO-doped β-Ga_2O_3 nanostructure photocatalysts. The absorption spectra of a solution of 30 ppm CR in presence of photocatalysts (*i.e.*, G, GC-1, GC-2, GC-3 and GC-5) under UV light irradiation are displayed in Fig. S2(a–e).† For the G sample, the maximum percent removal of CR is roughly 59.4% under UV light irradiation for 120 min. On the other hand, there is a small change in the CR concentration in the solution with the rod-like gallia sample. Introducing 1 to 5 wt% CoO increases the percent removal of CR to the range of 62.5–99.7%. As the CoO content was raised up to 3 wt%, the removal efficiency of CR improved. For GC-5 sample, percent removal remains almost constant. Nonetheless, there is a slightly difference in their removal times (Fig. S2† and Table 1). The maximum percent removal occurs in the GC-3 sample, and is measured to be 99.7% after approximately 75 min. Our results verified that removal of CR in GC photocatalysts is greater relative to pure gallia.

The photocatalytic performance could be ascribed to high surface area, value of band gap and differences in the rate of recombination, crystallinity of a photocatalyst, morphology, low degree of agglomeration, type of polymorph and lattice structure, defects (especially oxygen vacancies), and adsorptive affinity.[13,32] According to the BET and XRD results, presence of CoO was the main factor that enhanced the photoactivity of gallia. An increase in surface area of the samples raised the number of available surface active sites, which in turn caused

Table 2 Kinetics equation of photocatalytic degradation of CR

Samples	Order(s)	K_1 (min^{-1})	R_0	R_1	R_2
G	$\ln(C_0/C) = 0.0072t - 0.0345$	0.0072	0.0058	0.9904	0.9837
GC-1	$\ln(C_0/C) = 0.0086t - 0.0539$	0.0086	0.0237	0.9923	0.9609
GC-2	$\ln(C_0/C) = 0.012t - 0.081$	0.012	0.0864	0.9786	0.9022
GC-3	$\ln(C_0/C) = 0.0651t - 0.2225$	0.0651	0.1395	0.9878	0.85
GC-5	$\ln(C_0/C) = 0.0602t - 0.5233$	0.0602	0.23	0.9701	0.9336

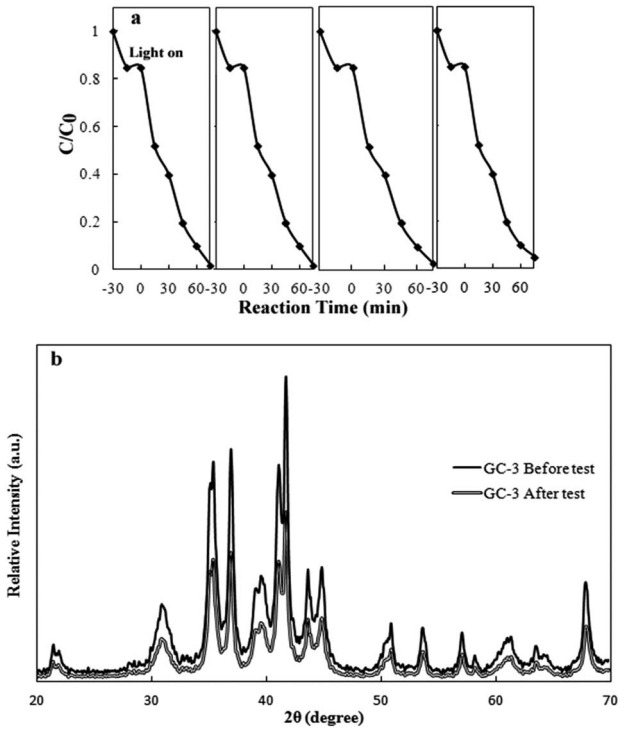

Fig. 6 Cycling run in the photodecoloration of CR in presence of GC-3 sample under UV light irradiation (a) and XRD pattern of GC-3 before and after photocatalytic test (b).

the adsorption of more dye molecules on the surfaces of photocatalysts.

To the best of our knowledge there is no evidence that $CoGa_2O_4$ and α-Ga_2O_3 are used as a photocatalyst for removal of pollutants. $CoGa_2O_4$ is a mixed oxide formed of two metal oxides as follows:

$$2CoGa_2O_4 \rightarrow 2Ga_2O_3 + 2CoO \quad (3)$$

A sharp increase in the SSA is observed for GC-3 compared to pure gallia. Also, PL spectra show that the recombination rate for GC-3 is lower than that for other samples. Appropriate reduction of the band gap energy and presence of two phases of $CoGa_2O_4$ and β-gallia have a major role in reduction of recombination rate. As a result, GC-3 shows maximum efficiency for degradation of CR.

Generally, the synergic effects of two parameters mentioned above (SSA and presence of two phases of $CoGa_2O_4$ and α-Ga_2O_3) by addition of cobalt(II) oxide up to 3–5 wt%, may lead to further enhancement of the photocatalytic activity of the GC-3 and GC-5 samples.

Kinetics of photocatalytic degradation of CR. In order to know the kinetics of photocatalytic degradation of CR in the solutions suspended on GC-*x* samples in Fig. S3,† different kinds of kinetics orders are attempted expressing the reaction kinetics as shown in Table 2. Each correlation coefficient was calculated from the kinetics equation, where R_0, R_1 and R_2 represent the correlation coefficients of zero, first and second order rate equations, respectively. Comparison between these correlation coefficients shows that R_1 has the best correlation for the different photocatalysts in Table 2. Therefore, it is suggested that the photocatalytic degradation of CR in the solutions suspended on CoO-loaded Ga_2O_3 samples belongs to first order reaction kinetics. From Table 2 it is seen that the K_1 values, rate constant of first order reaction kinetics, are in good agreement with the results of photocatalytic degradation of CR in Fig. S2† and Table 1.

Kinetic of the total mineralization of the dye. Fig. S4† presents the COD values for the best photocatalysts (GC-3 sample). As illustrated in this figure, the COD value of the initial color solution drastically diminishes after 80 h, indicating the great potential of GC-3 photo-degradation process for the removal of CR from wastewater. The photo-degradation efficiency was found to be 82.5% after 80 h in presence of 30 ppm of CR. Turnover number is defined as [(moles of decomposed pollutant)/(initial mole of the catalyst)].[33,34] In this work, after 80 h of irradiation, 82.5% of the initial CR was decomposed by GC-3, corresponding to turnover numbers of about 1.3. Additionally, GC-3 photocatalyst was very stable during four repeated experiments (Fig. 6a). The XRD patterns of the GC-3 photocatalyst before and after repeating the reaction for four cycles are displayed in Fig. 6b. This figure obviously proves that the structure of photocatalyst remains intact and no adsorption takes place on its surface. However, the diffraction intensity is reduced due to a decrease in the crystallinity of the sample. A similar observation has been reported by others.[35,36]

Conclusions

Photocatalytic activity of CoO-dopeed β-Ga_2O_3 nanostructures containing various proportions of CoO in presence of 30 ppm CR was investigated. The photocatalysts are successful not only in decolorization, but also in degradation and mineralization. The organic part was converted into mineral compounds as testified by the elimination of COD. The photocatalysts show maximum percent removal at RT, depending on the CoO

content, type of phase and SSA value. DRS UV-vis showed significant reduction in band gap upon increasing in their CoO content, indicating incorporation of CoO in gallia lattice. Therefore, presence of two phases of $CoGa_2O_4$ and α-Ga_2O_3 in GC-3 and GC-5 samples, respectively gives β-gallia a greater photocatalytic efficiency. The sample containing 3 wt% CoO shows the highest photocatalytic efficiency after 75 min of UV irradiation. Furthermore, photocatalytic activity of the sample containing 5 wt% of CoO tends to remain almost constant. Nonetheless, there is a slight difference in their removal times. The photocatalytic degradation of CR in the solution is quite consistent with first order reaction kinetics. Our findings may provide some insight into the preparation of the photocatalysis with superior performance in practical applications.

Acknowledgements

Financial support of this work by Tarbiat Modares University and University of Tehran is gratefully acknowledged.

Notes and references

1 S. Erdemoğlu, S. K. Aksu, F. Sayılkan, B. İzgi, M. Asiltürk, H. Sayılkan, F. Frimmel and Ş. Güçer, *J. Hazard. Mater.*, 2008, **155**, 469–476.
2 J. Wang, Y. Jiang, Z. Zhang, G. Zhao, G. Zhang, T. Ma and W. Sun, *Desalination*, 2007, **216**, 196–208.
3 K. Melghit, M. S. Al-Rubaei and I. Al-Amri, *J. Photochem. Photobiol., A*, 2006, **181**, 137–141.
4 H. Lachheb, E. Puzenat, A. Houas, M. Ksibi, E. Elaloui, C. Guillard and J.-M. Herrmann, *Appl. Catal., B*, 2002, **39**, 75–90.
5 V. A. Sakkas, M. A. Islam, C. Stalikas and T. A. Albanis, *J. Hazard. Mater.*, 2010, **175**, 33–44.
6 M. Dakiky and I. Nemcova, *Dyes Pigm.*, 2000, **44**, 181–193.
7 M. Y. Masoomi and A. Morsali, *RSC Adv.*, 2013, **3**, 19191–19218.
8 M. Y. Masoomi and A. Morsali, *Coord. Chem. Rev.*, 2012, **256**, 2921–2943.
9 B. Zhao and P. Zhang, *Catal. Commun.*, 2009, **10**, 1184–1187.
10 D.-Y. Wang, H.-C. Lin and C.-C. Yen, *Thin Solid Films*, 2006, **515**, 1047–1052.
11 Z. L. H. Xue, L. Wu, Z. Ding, X. Wang and X. Fu, *J. Phys. Chem. C*, 2008, **112**, 5850.
12 H. Xiao, H. Pei, J. Liu, J. Cui, B. Jiang, Q. Hou and W. Hu, *Mater. Lett.*, 2012, **71**, 145–147.
13 Y. Hou, L. Wu, X. Wang, Z. Ding, Z. Li and X. Fu, *J. Catal.*, 2007, **250**, 12–18.
14 X. Wang, S. Meng, X. Zhang, H. Wang, W. Zhong and Q. Du, *Chem. Phys. Lett.*, 2007, **444**, 292–296.
15 J. Zhang, D. Fu, H. Gao and L. Deng, *Appl. Surf. Sci.*, 2011, **258**, 1294–1299.
16 Y. Wang, J. Zhang, L. Liu, C. Zhu, X. Liu and Q. Su, *Mater. Lett.*, 2012, **75**, 95–98.
17 S. Kaur and V. Singh, *Ultrason. Sonochem.*, 2007, **14**, 531–537.
18 Y.-F. Wang, M.-C. Hsieh, J.-F. Lee and C.-M. Yang, *Appl. Catal., B*, 2013, **142–143**, 626–632.
19 H. R. Pouretedal and M. Kiyani, *J. Iran. Chem. Soc.*, 2014, **11**, 271–277.
20 M. Kim, *Korean J. Chem. Eng.*, 2005, **22**, 839–843.
21 Standard Methods for the Examination of Water and Wastewater, 5220 B CHEMICAL OXYGEN DEMAND (COD) Open Reflux Method, American Public Health Association, 20th edn, 1997.
22 R. Shannon, *Acta Crystallogr., Sect. A: Cryst. Phys., Diffr., Theor. Gen. Crystallogr.*, 1976, **32**, 751–767.
23 R. Al Asmar, J. P. Atanas, Y. Zaatar, J. Podlecki and A. Foucaran, *Microelectron. J.*, 2006, **37**, 1080–1085.
24 M. Bagheri, A. A. Khodadadi, A. R. Mahjoub and Y. Mortazavi, *Sens. Actuators, B*, 2013, **188**, 45–52.
25 M. Bagheri, A. R. Mahjoub and B. Mehri, *RSC Adv.*, 2014, **4**, 21757–21764.
26 Y. Luo, Z. Hou, J. Gao, D. Jin and X. Zheng, *Mater. Sci. Eng., B*, 2007, **140**, 123–127.
27 Y. Zhang, J. Yan, Q. Li, C. Qu, L. Zhang and W. Xie, *Mater. Sci. Eng., B*, 2011, **176**, 846–849.
28 Y. Hou, J. Zhang, Z. Ding and L. Wu, *Powder Technol.*, 2010, **203**, 440–446.
29 M. Bagheri, N. F. Hamedani, A. R. Mahjoub, A. A. Khodadadi and Y. Mortazavi, *Sens. Actuators, B*, 2014, **191**, 283–290.
30 G. Cao, *Nanostructures and nanomaterials Synthesis, Properties and Applications*, Imperial College Press, London, 2004.
31 R. Rahimi, H. Kerdari, M. Rabbani and M. Shafiee, *Desalination*, 2011, **280**, 412–418.
32 Q. Zhang, Y. Li, E. A. Ackerman, M. Gajdardziska-Josifovska and H. Li, *Appl. Catal., A*, 2011, **400**, 195–202.
33 H. Hori, A. Yamamoto, K. Koike, S. Kutsuna, M. Murayama, A. Yoshimoto and R. Arakawa, *Appl. Catal., B*, 2008, **82**, 58–66.
34 H. Hori, Y. Takano, K. Koike, S. Kutsuna, H. Einaga and T. Ibusuki, *Appl. Catal., B*, 2003, **46**, 333–340.
35 J. Zhang, A. V. Biradar, S. Pramanik, T. J. Emge, T. Asefa and J. Li, *Chem. Commun.*, 2012, **48**, 6541–6543.
36 J. Park, J.-R. Li, Y.-P. Chen, J. Yu, A. A. Yakovenko, Z. U. Wang, L.-B. Sun, P. B. Balbuena and H.-C. Zhou, *Chem. Commun.*, 2012, **48**, 9995–9997.

